XI International Conference on Computational Plasticity. Fundamentals and Applications
COMPLAS XI
E. Oñate, D.R.J. Owen, D. Peric and B. Suárez (Eds)

NUMERICAL INVESTIGATIONS OF MECHANICAL STRESS CAUSED IN DENDRITE BY MELT CONVECTION AND GRAVITY

H. Kashima*, T. Takaki†, T. Fukui† and K. Morinishi†

* Mechanical and system Engineering
Kyoto Institute of Technology
Matsugasaki, Sakyo, Kyoto, 606-8585, Japan
e-mail: m0623012@kit.ac.jp

† Mechanical and system Engineering
Kyoto Institute of Technology
Matsugasaki, Sakyo, Kyoto, 606-8585, Japan
e-mail: takaki@kit.ac.jp, www.cis.kit.ac.jp/~takaki/

Key words: Dendrite, Fragmentation, Solidification, Melt Convection, Stress, Phase-Field Method, Navier-Stokes Equations, Finite Element Method.

Abstract. In order to investigate the effects of stress around dendrite neck cased by the convection and gravity on the dendrite fragmentation, the novel numerical model, where phase-field method, Navier-Stokes equations and finite element method are continuously and independently employed, has been developed. By applying the model to the dendritic solidification of Al-Si alloy, the maximum stress variations by melt convection and gravity with dendrite growth were evaluated.

1 INTRODUCTION

Dendrite plays especially important role for formation of solidification microstructure of metallic alloy, because it determines the size and shape of solidified grains. Therefore, it is essential for high quality casting to predict and control the dendritic morphology with high accuracy.

In casting, the final microstructure in the ingot is formed through two different dendritic growths. One is columnar structure, in which the dendrites grow preferentially oriented perpendicular to the mold walls, and the other is equiaxed structure, in which the dendrites grow in all space directions. In particular, the equiaxed grain structure has a dominant influence on the mechanical characteristics of casting product, because it controls the size of solidification microstructure. One of the sources of the equiaxed grains is thought to be the dendrite fragmentations caused in columnar region.

It is reported that the dendrite fragmentation occured by local remelting and the mechanical fragmentation due to the melt flow is not important for grain refinement [1] except for rapid solidification [2]. Recently, studies using in-situ and real-time observations reported that the mechanical stress caused by the melt convection and the gravity promotes the dendrite fragmentation [3]. However, its detail mechanism is not yet elucidated.

In this study, in order to reveal the effects of mechanical stress caused by the convection

and gravity on dendrite fragmentation, we developed a new simulation model and investigate the stress in dendrite neck. The coupling simulations by phase-field method, Navier-Stokes equations and finite element method are performed. In this simulation, first, realistic dendritic morphologies are simulated by phase-field method and, successively, the flow fields around the dendrite are simulated by Navier-Stokes equations. Lastly, the stresses in dendrite caused by melt convection and gravity are calculated by finite element method. The variations of maximum stress occurred at the dendrite neck with dendrite growth are discussed.

2 NUMERICAL PROCEDURE AND MODELS

2.1 Numerical procedure

The dendritic growth of Al-Si alloy and the flow field of solution around the dendrite in forced flow are simulated. And then, the stresses in dendrite caused by the flow and gravity are calculated. The calculations are performed in the order of phase-field method, Navier-Stokes equation and finite element method.

At first, the dendrite morphologies during solidification of Al-Si alloy are simulated by the phase-field method. Next, the fluid flow around the dendrite is simulated by using two-phase Navier-Stokes equations and the pressure distributions acting on the dendrite surface are calculated. Lastly, the stress distributions in the dendrite caused by the fluid flow and gravity are simulated by using finite element method. In the following, the phase-field model and the two-phase Navier-Stokes equation are explained in detail.

2.2 Phase-field model

The dendritic growth of Al-Si alloy in isothermal condition is simulated by the phase-field method. The evolution equation of phase field variable ϕ, which takes 1 in a solid and 0 in a liquid, is expressed by

$$\frac{\partial \phi}{\partial t} = M_\phi \left[\nabla (a^2 \nabla \phi) - \frac{\partial}{\partial x}\left(a \frac{\partial a}{\partial \theta} \frac{\partial \phi}{\partial y} \right) + \frac{\partial}{\partial y}\left(a \frac{\partial a}{\partial \theta} \frac{\partial \phi}{\partial x} \right) + 4W\phi(1-\phi)(\phi - 0.5 + \beta) \right], \quad (1)$$

where, τ is the time and a is the gradient coefficient considering interface anisotropy by the equation $a(\theta) = \bar{a}\{1 + \zeta \cos(k\theta)\}$, where θ is the angle between x-axis and interface normal, ζ is the strength of anisotropy and κ is the anisotropy mode of κ=4. β in the Eq. (1) is expressed by

$$\beta = -\frac{15}{2W}\phi(1-\phi)\Delta S(T - T_m(c)). \quad (2)$$

Here, ΔS is the transformation entropy, T is the temperature, Tm is the temperature on the linearized liquidus line expressed by $T_m = m_L c + T_r$, where mL is the liquidus slope, c is the

solute concentration, *Tr* is a reference temperature. In addition, $\bar{a}$, W and M_ϕ in Eq.(1) can be related to the material parameters by following equations:

$$\bar{a} = \sqrt{\frac{3\delta\gamma}{b}},\ W = \frac{6\gamma b}{\delta},\ M_\phi = \frac{\sqrt{2W}}{6a}M\ , \tag{3}$$

where, δ is the interface thickness, γ is the interface energy, M is the interface mobility, and $b = 2\tanh^{-1}(1-2\lambda)$ is a constant related to interface thickness, where $\lambda = 0.1$ is employed. The concentration *c* in Eq.(2) is calculated by the following diffusion equation

$$\frac{\partial c}{\partial t} = \nabla D\left[\nabla c + \frac{(1-k)c}{1-\phi+k\phi}\nabla\phi\right], \tag{4}$$

where, *k* is the partition coefficient given by $k = cs/c_L$, where *cs* and *cL* are the concentrations in solid and liquid, respectively. The concentration *c* is defined by

$$c = \phi c_S + (1-\phi)c_L\ . \tag{5}$$

Diffusion coefficint *D* in Eq.(4) is indicated by

$$D = D_s + (D_L - D_S)\frac{1-\phi}{1-\phi+k\phi}, \tag{6}$$

where, *Ds* and *DL* are diffusion coefficients of solid and liquid, respectively.

2.3 Two-phase Navier-Stokes model

The melt convection around dendrite in forced flow is simulated by the following two-phase Navier-Stokes equations using phase-field parameter [4, 5].

$$\frac{\partial(1-\phi)u}{\partial x} + \frac{\partial(1-\phi)v}{\partial y} = 0\ . \tag{7}$$

$$\frac{\partial(1-\phi)u}{\partial t} + u(1-\phi)\frac{\partial u}{\partial x} + v(1-\phi)\frac{\partial u}{\partial y} = -\frac{1}{\rho}(1-\phi)\frac{\partial p}{\partial x} + \nu\left(\frac{\partial^2(1-\phi)u}{\partial x^2} + \frac{\partial^2(1-\phi)u}{\partial y^2}\right) + F_{dx}\ . \tag{8}$$

$$\frac{\partial(1-\phi)v}{\partial t} + u(1-\phi)\frac{\partial v}{\partial x} + v(1-\phi)\frac{\partial v}{\partial y} = -\frac{1}{\rho}(1-\phi)\frac{\partial p}{\partial y} + \nu\left(\frac{\partial^2(1-\phi)v}{\partial x^2} + \frac{\partial^2(1-\phi)v}{\partial y^2}\right) + F_{dy}\ . \tag{9}$$

Here, u and v are velocities in x and y direction, respectively. ρ is the flow density, p is the pressure, and ν is the kinetic viscosity. Note that, in the liquid of $\phi = 0$, Eqs. (7) - (9) reduce to the normal single-phase Navier-Stokes equations for a Newtonian fluid with a constant density and viscosity. The last term on the right hand side of Eq.(8) and Eq.(9), or F_{dx} and F_{dy}, are employed to account for the dissipative viscous stress in the liquid due to interactions with the solid in the diffuse interface region and expressed by

$$F_{dx} = \mu_L \frac{h_d \phi^2 (1-\phi)}{\Delta^2} u \,, \tag{10}$$

$$F_{dy} = \mu_L \frac{h_d \phi^2 (1-\phi)}{\Delta^2} v \,, \tag{11}$$

where, μ_L is the kinetic coefficint, Δ is the thickness of interface which is expressed by $\Delta = \delta / \Delta x$, where Δx is the lattice size. The *hd* is a dimensionless constant which is determined by numerical experiment.

3 NUMRICAL RESULTS

3.1 Dendritic growth simulations by phase-field method

By coupling Eq.(1) and Eq.(4), dendritic growths of Al-Si alloy under isothermal condition are simulated. Figure 1 shows the computational domain and initial conditions.

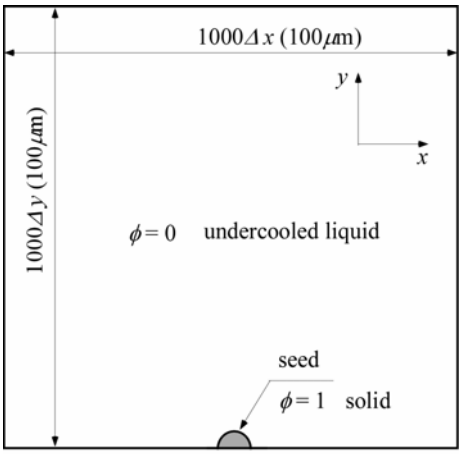

Figure 1 : Computational domain and boundary conditions
for dendritic growth simulation by phase-field method

Initially, all regions are filled with the undercooled liquid ($\phi = 0$), and temperature and concentration is set to be T = 886 K and c = 0.06, respectively. To simulate the dendritic growth from the bottom of computational domain which images the mold wall, one semicircle seed with radius $6\Delta x$ is putted on the bottom of the region. Computational domain with 100μm×100μm is divided into 1000×1000 finite different lattices. Therefore, the lattice size $\Delta x = \Delta y$ is to be 100 nm. The zero Neumann boundary conditions are employed on all boundaries for both ϕ and c. In the present simulations, we focus on the growth of first dendrite arm. Therefore, the concentration fluctuation which is usually used in the dendritic

growth simulation to form second arm is not taken into consideration. The employed material parameters for Al-Si alloy are shown in Table1.

Table 1 : Physical properties

Partition coefficient k	0.13
Reference temperature T_r [K]	933.47
Liquidus slope m_L [K/mol. fract.]	-600
Diffusion coefficient of liquid D_L [m^2/s]	1.0×10^{-12}
Diffusion coefficient of solid Ds [m^2/s]	3.0×10^{-9}
Interface energy γ [J/m^2]	0.16
Transformation entropy ΔS [JK/m^3]	8.0×10^{5}
Interface thickness δ [m]	$6\Delta x$
Interface mobility M [m^4/Js]	0.03

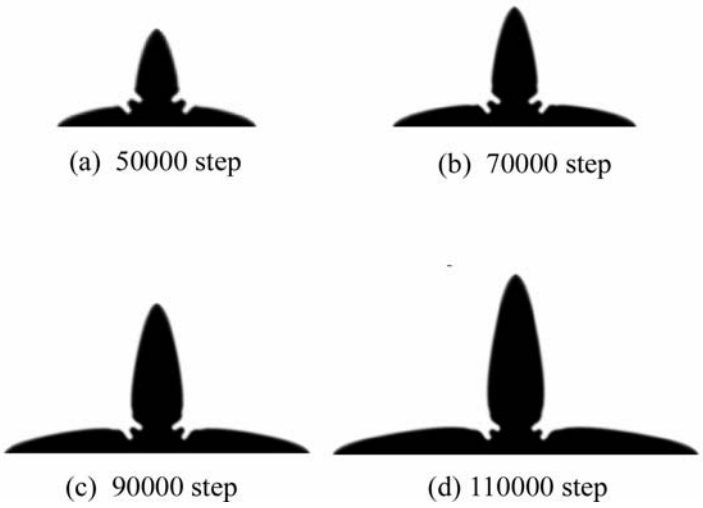

Figure 2 : Variations of dendrite morphologies

Figure 2 shows the numerical results of dendrite growth process during solidification simulation. It is observed that Al-Si alloy dendirte grows keeping the thin shape and the width of the thinest portion of dendrite neck is almost constant during growth. Therefore, it is concluded that the Al-Si dendrite has a shape which easily cause the stress concentration at the dendrite neck by the convection and gravity.

3.2 Fluid flow simulations around dendrite by two-phase Navier-Stokes equations

Next, the melt convection around the dendrite shown in Fig. 2 is calculated by using two-phase Navier-Stokes equations of Eqs.(7) - (9). Then, those equations are solved by artificial compressibility method [6], where the inertial term is discretized by third-order weighted ENO scheme and the viscous term is computed by using second-order accurate central-difference scheme.

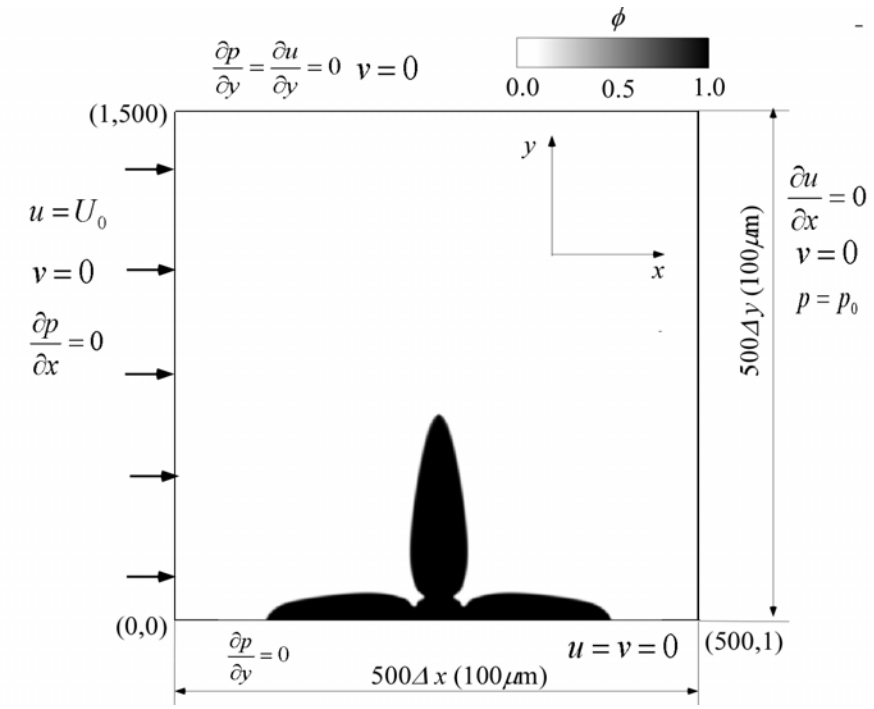

Figure 3 : Computational domain and initial conditions for simulation of melt convection around the dendrite

Figure 3 shows the computational domain and boundary conditions. The uniform forced flow *U0*= 0.01 m/s, which is normal melt flow velocity in casting [7], is applied on the left side of the domain and the pressure on the right side are fixed to $p_0 = \rho U02$ [Pa]. The other boundary conditions are shown in Fig.3. Reynolds number is set to be Re = 5. The dimensionless constant hd in Eq.(10) and Eq.(11) was determined as $hd = 5.0\times10^6$ by performing numerical experiments so as that the fluid velocity at $\phi = 0.5$ is to be zero. For reducing the computational cost, the coarse finite difference lattices of 500×500 (Δx = 200 nm) are employed.

Numerical results at steady-state condition are shown in Figs. 4 and 5. Figure 5 shows the fluid flow velocities by both color and vectors and Fig. 4 shows pressure distributions. In both figures, figures (a), (b), (c) and (d) correspond to those of Fig. 2. From Fig.4, the vortex occurred at the right side of dendrite becomes larger as the dendrite grows. Therefore, the negative pressure is generated at the right side of dendrite. On the left surface of dendrite, the compressive pressures are generated and its magnitude increases with growing the dendrite. The fluid pressures acting on the dendrite surface are transferred to the next stress simulation.

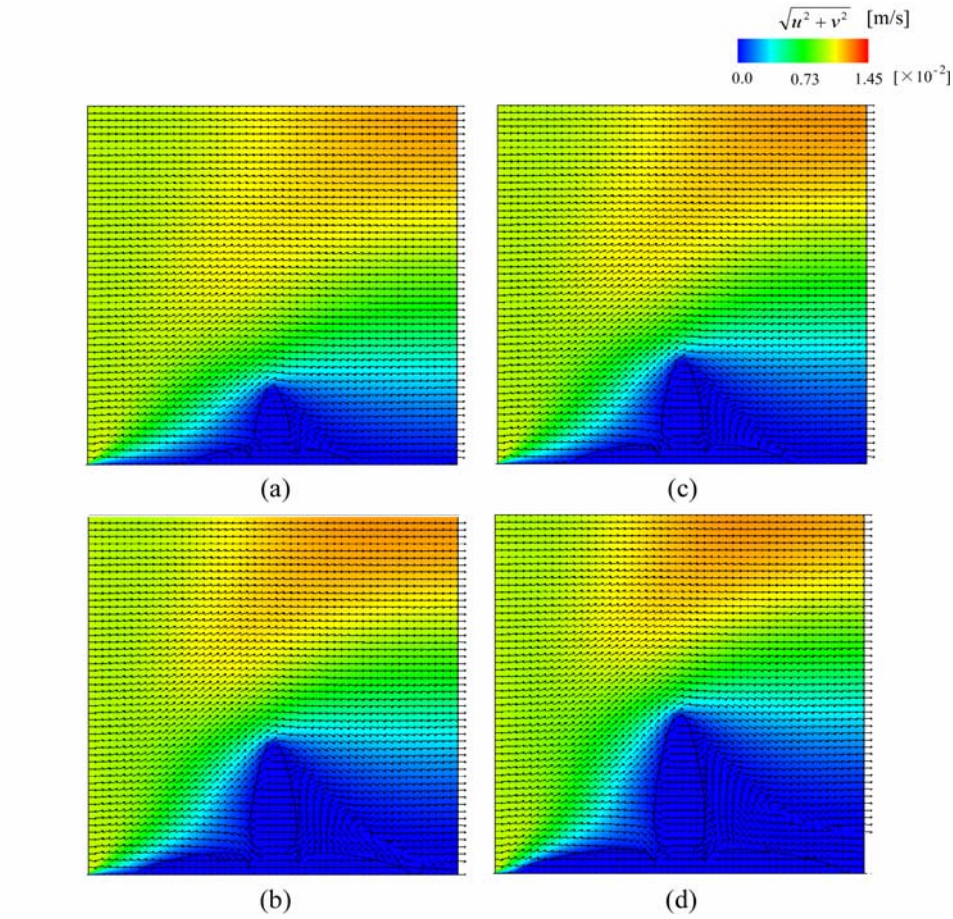

Figure 4 : Variations of fluid flow velocity with dendrite growth

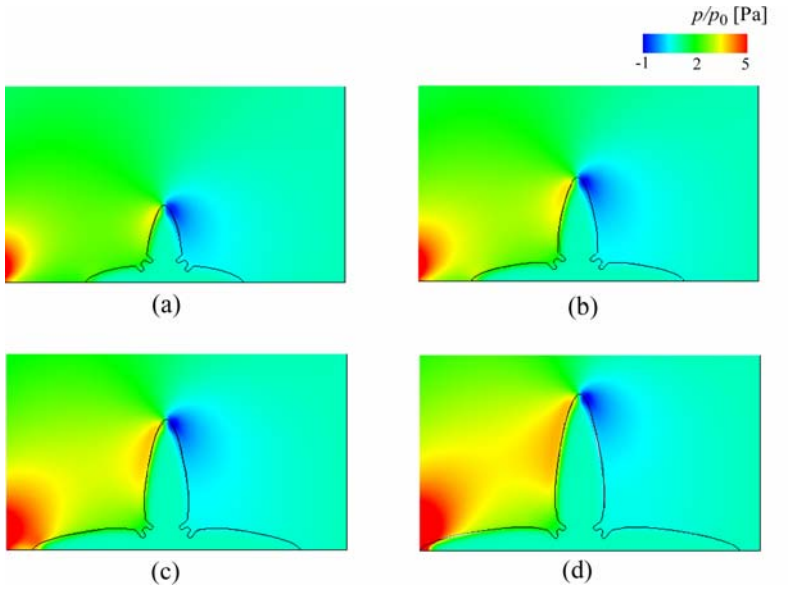

Figure 5 : Variations of pressure distribution with dendrite growth

3.3 Finite element simulations of stress in dendrite

The stresses in dendrite caused by the convection calculated in the previous section and the gravity which acts in vertical direction of dendrite first arm are simulated by finite element method using four node isoparametric elements as plane stress problem.

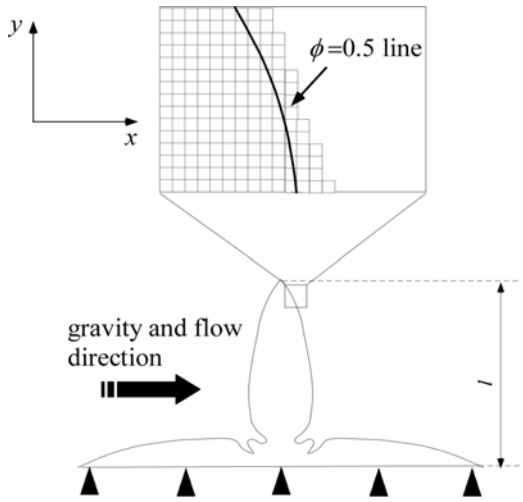

Figure 6 : Computational domain and boundary conditions for finite element simulation to calculate stress field in dendrite

Figure 6 shows the computational domain and boundary conditions. From the results of phase-field simulation shown in Fig. 2, the finite difference lattices with $\phi > 0.1$ are taken out and are used as elements for the stress evaluation by finite element method. In the interface, the Young's modulus is set to change smoothly as ϕE, where E is Young's modulus in solid phase. Both displacements in x and y directions on the bottom of the computational domain, which corresponds to the mold wall, are constrained. l shown in Fig.6 is the dendrite length. The pressure distributions on the dendrite surface caused by the convection are transformed to the nodal forces by following equations:

$$F_x = \phi(p - p_0)\Delta x \cos\theta, \tag{12}$$

$$F_y = \phi(p - p_0)\Delta y \sin\theta, \tag{13}$$

where, θ is the angle between x-axis and interface normal. Equations (12) and (13) are calculated in the range $0.1 < \phi < 0.5$ and the nodal forces are applied to the nodes having ϕ nearest to 0.5.

The body force due to gravity is introduced to all nodes by the nodal force calculated by

$$F_g = \phi\Delta x\Delta y(\rho_s - \rho_L)g, \tag{14}$$

where, ρ_s and ρ_L are the density in solid and liquid, respectively, and g is the gravitational acceleration. The employed material parameters using finite element method are as follows:

Young's modulus E = 4.5 GPa, Poisson's ratio ν = 0.3, the gravitational acceleration g = 9.8 m/s^2, the solid density $\rho_s = 2.68\times10^3$ kg/m^3 , and the liquid density $\rho_L = 2.4\times10^3$ kg/m^3 [8].

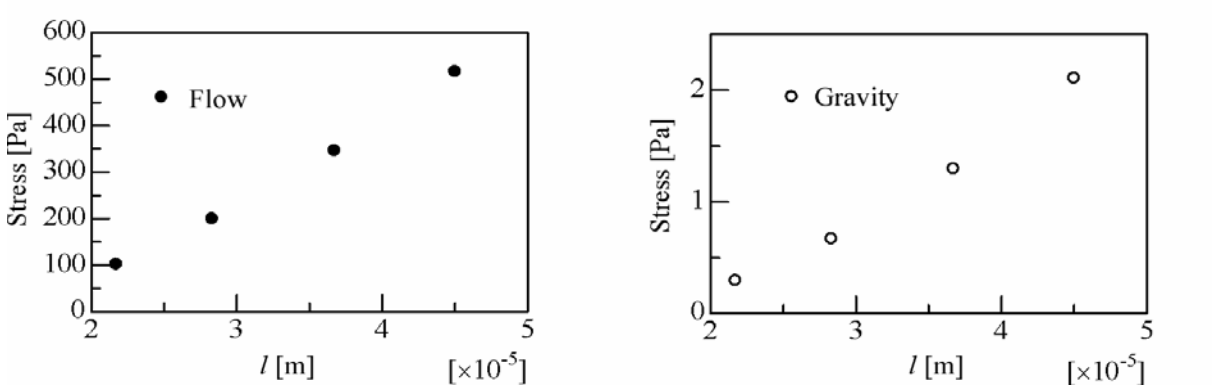

(a) Convection (b) Gravity

Figure 7 : Variations of maximum stress caused at dendrite neck by convection and gravity

Figure 7 shows the variations of maximum stress caused at dendrite neck by convection and gravity. The abscissa is the dendrite length l and the ordinate is the maximum equivalent stress. From Fig.7, the maximum stress by convection is much higher than that of gravity. In the present simulations, the forced flow is set to be 0.01 m/s which is normal melt flow velocity in casting. On the other hand, the most severe condition is set for the gravity, because the gravity acts in the perpendicular direction to the dendrite axis. Considering these points, it is concluded that the gravity has less influence on the fragmentation comparing to the melt convection. However, we need further investigations for larger dendrite with many secondary arms.

4 CONCLUSION

In order to investigate the effects of stress around dendrite neck cased by the convection and gravity on the dendrite fragmentation, the novel numerical model, where phase-field method, Navier-Stokes equations and finite element method are continuously and independently employed, has been developed. By applying the model to the dendritic solidification of Al-Si alloy, the maximum stress variations by melt convection and gravity with dendrite growth were evaluated. As a result, it was concluded that the convection is more important for the maximum stress in dendrite than the gravity.

REFERENCES

[1] J. Pilling and A. Hellawell, Mechanical deformation of dendrites by fluid flow, *Metal. Mater. Trans. A,* (1996) **27**:229-232.

[2] A. M. Mullis, D. J. Walkers, S.E. Battersby and R. F. Cochrane, Deformation of dendrites by fluid flow during rapid solidification, *Mater. Sci. Eng. A*, (2001) **304-306**:245-249.

[3] G. Reinhart, A. Buffet, H. Nguyen-Thi, B. Billia, H. Hung, N. Mangelick-Noël, N. Bergeon, T. Schenk, J. Härtwing and J. Baruchel, In-situ and real-time analysis of the formation of strains and

microstructure defects during solidification of Al-3.5 Wt Pct Ni alloys, *Metal. Mater. Trans. A*, (2008) **39**:865-874.

[4] J. Ni and C. Beckermann, A Volume-Averaged Two-Phase Model for Solidification Transport Phenomena, *Metall. Trans. B*, (1991) **22**:349-361.

[5] C. Beckermann, H.-J. Diepers, I. Steinbach, A. Karma and X. Tong, Modeling melt convection in phase-field simulations of solidification, *J. Compu. Phys*., (1999) **154**:468-496.

[6] T. Miyake, H. Tokunaga, N. Satofuka, Explicit time accurate pseudo-compressibility method for numerical solutions of unsteady incompressible viscous flows, *Eng. Mech. Soc. Jpn. Trans. B*, (1993) **59**:36-42. (in Japanese)

[7] H. Takatani, Ch.-A. Grandin and M. Rappaz, EBSD characterisation and modelling of columnar dendritic grains growing in the presence of fluid flow, *Acta. Mater.*, (2000) **59**:675-688. (in Japanese)

[8] The Japan institute of metals, *Kinnzoku deta bukku.* Maruzen, Vol. II., (1999) 67-68. (in Japanese)